ACS APPLIED POLYMER MATERIALS

Article

Cite This: ACS Appl. Polym. Mater. 2019, 1, 2943−2950

pubs.acs.org/acsapm

Chemical Doping of Well-Dispersed P3HT Thin-Film Nanowire Networks

Kan Tang,[†] Lifeng Huang,[‡] Jasmine Lim,[‡] Trishal Zaveri,[†] Jason D. Azoulay,[‡] and Song Guo*[,†]

[†]Department of Chemistry and Biochemistry and [‡]Center for Optoelectronic Materials and Devices, School of Polymer Science and Engineering, The University of Southern Mississippi, Hattiesburg, Mississippi 39406, United States

Supporting Information

ABSTRACT: We demonstrate the preparation of uniformly distributed poly(3-hexylthiophene) (P3HT) nanowire (NW) networks on a variety of substrates. We studied changes in the optical, electronic, and morphological properties upon sequential doping by 2,3,5,6-tetrafluoro-7,7,8,8-tetracyanoquinodimethane (F4TCNQ) by UV−vis spectroscopy, atomic force microscopy (AFM), Kelvin probe force microscopy (KPFM), and electrical conductivity measurements. At a moderate dopant concentration of 250 μg/mL, the P3HT NW networks retain their morphological features with a clear evolution of an absorption band corresponding to doping products. Higher dopant concentrations (∼1 mg/mL) lead to the accumulation of dopant molecules on the surface of the film, forming "dot-like" features. KPFM measurements show a clear difference in the contact potential difference (CPD) of the P3HT NWs with varying doping concentration regimes. Moreover, an increase in the electrical conductivity by 4 orders of magnitude from 10^{-5} to 10^{-1} S/cm is observed after moderate doping, demonstrating that significant doping effects can be achieved for a mostly crystalline phase of P3HT such as its nanowire form.

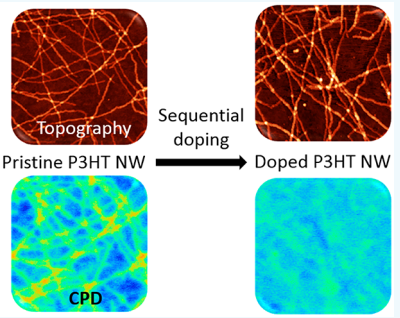

KEYWORDS: *conjugated polymers, chemical doping, nanowire network, Kelvin probe force microscopy, conductivity*

INTRODUCTION

The chemical doping of conjugated polymers (CPs) remains one of the most widely utilized methods to manipulate the optical and electronic properties of these materials and increase the electrical conductivity. This has resulted in a diversity of technologies such as field effect transistors (FETs),[1−3] organic light-emitting diodes (OLEDs),[4] and sensors[5] with numerous new applications continually emerging. Among methods of chemically doping CPs, solution-based methods offer low-cost, convenience, and compatibility with solution-processing methods most commonly utilized for device fabrication.[1−3] There are generally two solution-based approaches used to dope CPs. The first, mixed solution doping, constitutes the mixing of dopant molecules with the polymers before the formation of the active layer. However, because of the complex intermolecular interactions resulting from charge transfer between dopant molecules and CPs and the decreased solubility of the doped products, this method often leads to nonideal morphological characteristics upon film formation.[6,7] Another method, sequential doping, relies on the application of a dopant solution to the surface of the CP film. Sequential doping provides a valuable route to overcome the difficulties associated with processing doped poly(3-hexylthiophene) (P3HT) from solution and results in better film quality and enhanced electrical conductivity.[6−8]

P3HT is widely considered a benchmark material for use in organic electronic devices such as organic photovoltaics (OPVs)[9] and organic field-effect transistors (OFETs).[10−12] Despite the extensive studies performed with P3HT as a semiconductor in a variety of applications, there are still a relatively limited number of studies related to P3HT nanowire (NW) structures. These structures can be accessed via controlled seeding,[13−15] electric-field-assisted alignment,[16−20] or electrospinning.[21−26] The "whisker method" provides high-aspect-ratio P3HT nanofibers, which crystallize from "poor" solvents.[27] P3HT NW samples can be prepared via solution deposition of aggregated P3HT nanowhiskers onto a suitable substrate by solution casting methods,[28−36] which often lead to heterogeneous coverage of NWs on surfaces. The characterization of isolated P3HT NWs has been previously reported.[37−41] Despite the significance of understanding the fundamental electrical properties of isolated NWs, the extensive lithographic techniques involved in accessing these structures hinder practical device applications and provide a limited understanding of their ensemble optoelectronic properties. To utilize P3HT NW networks in optoelectronic devices, a more uniform distribution of P3HT NWs on the surface is preferred.[42,43]

Here, we demonstrate that P3HT NW networks can be prepared by spin-coating a P3HT nanowhisker solution formed at a low P3HT concentration of 60 μg/mL. Doping of the nanowire network is performed by using 2,3,5,6-

Received: July 16, 2019
Accepted: September 24, 2019
Published: September 24, 2019

DOI: 10.1021/acsapm.9b00653
ACS Appl. Polym. Mater. 2019, 1, 2943−2950

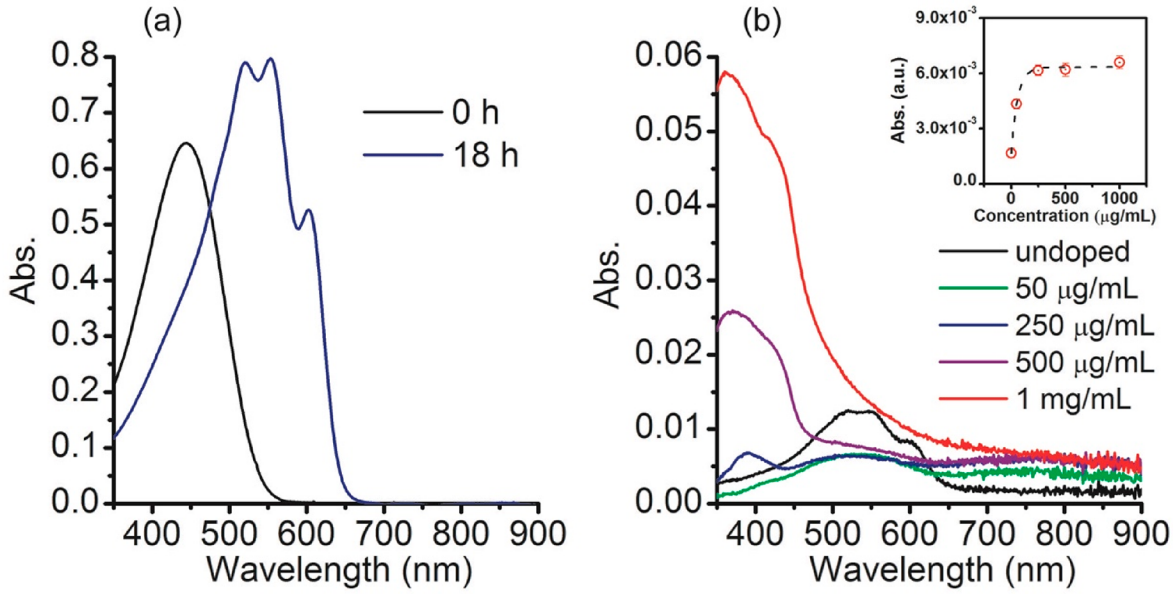

Figure 1. (a) UV−vis absorption spectra of P3HT in 4:1 (v/v) anisole/chloroform solvent in the fully solubilized state (t = 0 h, T = 90 °C) and aggregated state (t = 18 h, T = 25 °C). Note that the cooling rate was 25 °C/h, and the temperature was held constant once 25 °C was reached. (b) UV−vis absorption spectra of P3HT NWs on glass slides. F4TCNQ solutions in acetonitrile with concentrations from 0 to 1 mg/mL were applied to the surface, resulting in the formation of a wide absorbance band above 650 nm that is attributed to P3HT polarons and F4TCNQ anions. Inset: absorbance at 768 nm as a function of dopant concentration.

tetrafluoro-7,7,8,8-tetracyanoquinodimethane (F4TCNQ), a prototypical p-type dopant for P3HT.[44−48] Results from atomic force microscopy (AFM) and Kelvin probe force microscopy (KPFM) measurements are used to distinguish undoped, moderately doped, and excessively doped P3HT NW networks and offer insight into their electronic properties. Furthermore, an increase in the electrical conductivity by 4 orders of magnitude from 10^{-5} to 10^{-1} S/cm is observed after moderate chemical doping of the P3HT NW networks.

EXPERIMENTAL SECTION

Materials. Solvents, unless otherwise specified, were purchased from Fisher Scientific and used without additional purification. Regioregular (RR) P3HT (M_n = 70.5 kDa, dispersity ($Đ$) = 1.7, head-to-tail (H−T) regioregularity >98%) was purchased from Sigma-Aldrich. F4TCNQ (>98%) was purchased from TCI America and used as received. Indium tin oxide (ITO)-coated glass substrates were purchased from Colorado Concept Coating, LLC, USA. Glass slides (2 cm × 2 cm × 0.17 mm) were purchased from Fisher Scientific, USA. Quartz substrates (S151) for conductivity measurements were purchased from Ossila, Ltd., UK.

Nanowire Preparation. 2.4 mg of RR-P3HT was added to 40 mL of an 4:1 (v/v) anisole/chloroform mixture.[42,43] The resultant 60 μg/mL P3HT solution was heated at 90 °C for 15 min until an orange solution was obtained. The P3HT solution was subsequently cooled to 25 °C at a rate of 25 °C/h controlled by a Quantum Northwest TC1 temperature controller and then aged at that temperature for 18 h. After aging, the orange-colored P3HT solution became purple, indicating the formation of NWs.

Characterization. UV−vis absorption spectra were recorded on an Agilent Cary 60 UV−vis spectrometer. For solution absorption measurements, P3HT was dissolved in a 4:1 (v/v) anisole/chloroform mixture at a concentration of 60 μg/mL and transferred into airtight custom-made cuvettes (2 mm optical path length). For solid-state absorption experiments, glass slides (0.17 mm thick) were cleaned by dipping in hot concentrated HNO_3 for 15 min, followed by rinsing in deionized water before use. An aged 60 μg/mL P3HT solution was spin-coated at 3000 rpm for 120 s to form P3HT NW networks. Doped samples were prepared by covering the P3HT-coated substrate with solutions of F4TCNQ in acetonitrile for 15 s. The liquid was subsequently removed from the surface by spinning at 2000 rpm for 30 s.

The 1 × 1 cm^2 ITO substrates were ultrasonicated in a 1:1:1 mixture of chlorobenzene, toluene, and acetone for 15 min and then heated at 90 °C for 15 min. Next, the substrates were soaked in toluene, which was previously filtered through a 0.25 μm pore size membrane filter and subsequently blown dry under a flow of nitrogen before use. The preparation of pristine and doped P3HT NWs on ITO substrates follows the same protocol as previously described on a glass substrate. AFM and KPFM measurements were performed on an NTEGRA Prima AFM from NT-MDT Spectrum Instruments. Both topography and KPFM images were collected using Pt-coated silicon tips (NSC18-Pt) from μMasch with a typical resonant frequency of 75 kHz and a spring force constant of 1.2−5.5 N/m. Topography imaging was performed using semicontact mode. Two-pass lift mode was used in KPFM measurements. The first KPFM pass was performed in semicontact mode. Tracing the recorded topography scan, a second pass with a lift height of 10 nm could resolve the contact potential difference (CPD) between the tip and surface features. The surface coverage (ϕ) of P3HT NW networks on the ITO substrate is determined by using the mark grains module in Gwyddion software (http://gwyddion.net/, Czech Metrology Institute). The difference in CPD values between P3HT NWs and the ITO region can be regarded as the difference in their work functions without concerning work function variations of the AFM tip.

Device Fabrication and Charge Transport Measurements. Quartz substrates were sequentially cleaned by ultrasonication in detergent (2% Hellmanex in deionized water), deionized water, acetone, and isopropyl alcohol for 15 min each followed by drying in an oven. Gold (Au) electrodes (60 nm) were thermally deposited on quartz at 10^{-6} Torr by using a patterned shadow mask, resulting in a well-defined channel length (L) of 30 μm and width (W) of 1 mm. Undoped and doped P3HT NW networks were prepared following the same protocol that was used for glass and ITO substrates. Devices were tested on a Signatone 1160 series probe station coupled to a Keithley 4200 semiconductor characterization system inside a nitrogen-filled glovebox. The conductivity of the P3HT NW networks was calculated from the expression

DOI: 10.1021/acsapm.9b00653
ACS Appl. Polym. Mater. 2019, 1, 2943−2950

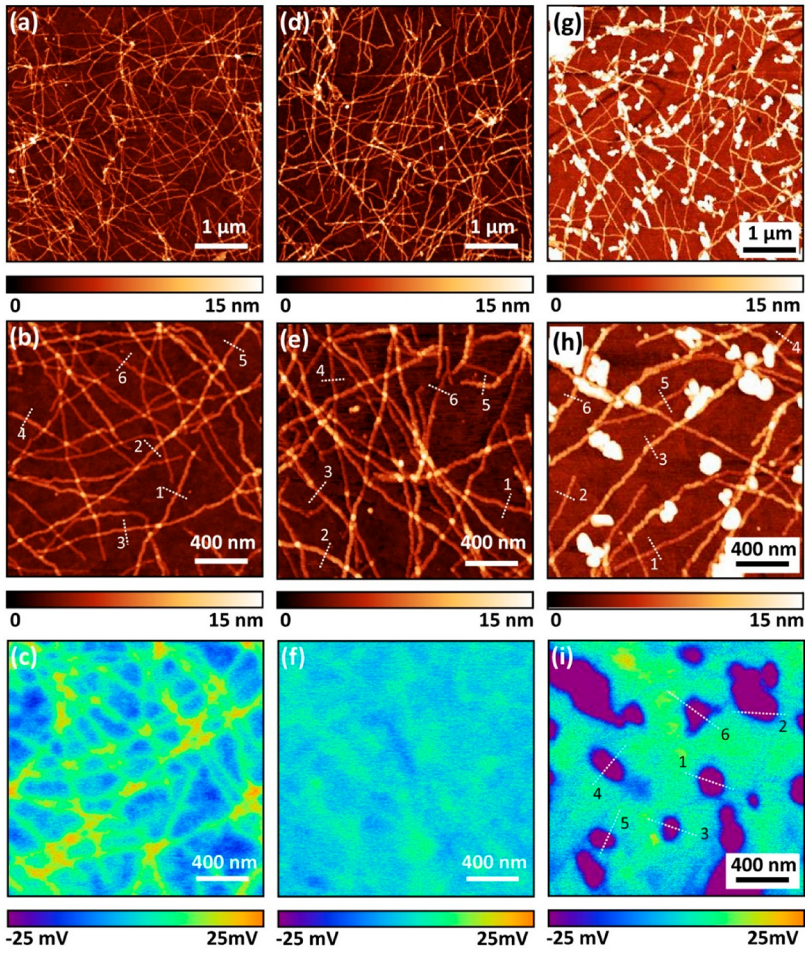

Figure 2. (a) AFM topography image of P3HT nanowires on ITO. A magnified 2 × 2 μm^2 image is shown in panel (b). The KPFM image of pristine P3HT NW network (c) presents a distinguishable 10 mV CPD contrast between NWs and the ITO substrate. Sequentially doped P3HT NWs with 250 μg/mL F4TCNQ retain the morphology of pristine NWs (d, e) while the average thickness of NWs increases. Noticeably, KPFM result in panel (f) shows CPD of NWs and ITO becomes indistinguishable. Upon 1 mg/mL F4TCNQ sequential doping of P3HT, irregular dot-like features associated with excessive neutral dopant emerge (g, h), showing significantly lower CPD values as compared to the doped NWs and the ITO substrate. The height profiles of marked cross sections (1−6) in panels (b) and (e) are summarized and can be found in Figure 3, while the CPD profiles of marked cross sections (1−6) in panel (i) can be referred to Figure S3.

$$\sigma = G\frac{L}{\phi W h_a}$$

where G is the conductance, L is the channel length, W is the channel width, and h_a is the average thickness/height of the NW network, respectively. G of each device is interpreted from the slope of its current−voltage (I−V) characteristic curve. ϕ is defined as the surface coverage of the P3HT nanowire networks. Note that the product ϕW can be regarded as the effective width of the network W_{eff} between two 30 μm channel length Au electrodes. For the undoped and doped samples, the reported conductivity was averaged from 10 devices.

RESULTS AND DISCUSSION

As shown in Figure 1a, an absorption maximum (λ_{max}) at 445 nm was observed for P3HT in a 4:1 (v/v) anisole/chloroform mixture corresponding to fully solubilized P3HT.[49−51] Following controlled aging at 25 °C, there is a bathochromic shift in the absorption profile with two peaks at 603 and 553 nm, which can be assigned as the 0−0 and 0−1 vibronic transitions of the P3HT aggregate, respectively.[52−54] After aging, no significant absorption peak can be observed at 445 nm. The A_{0-0}/A_{0-1} ratio indicates whether aggregates show H- or J-type character.[52−54] Here, a ratio of 0.66 corresponds to the formation of H-aggregates as $A_{0-0}/A_{0-1} < 1$. By assuming a Huang−Rhys factor of 1, the free exciton bandwidth (W) of the H-aggregate can be determined from the expression[52−54]

$$\frac{A_{0-0}}{A_{0-1}} \approx \left(\frac{1 - \frac{0.24W}{E_p}}{1 + \frac{0.073W}{E_p}}\right)^2$$

where E_p is the energy of dominating intramolecular C=C vibrations that are assumed to be at 0.18 eV.[55,56] The calculated W for the P3HT aggregate in this binary solvent is about 113 meV, comparable to the value of solid-state P3HT films prepared from low boiling point solvents such as chloroform.[51,57,58] The absorbance at 445 nm is reduced in intensity by 55% when compared to the fully solubilized P3HT, indicating the formation of 45% crystalline P3HT. Alternatively, the absorption spectra of aged P3HT solution can be deconvoluted into a combination of fully solubilized absorption band $A_{s\text{-}P3HT}$ and aggregate absorption $A_{NW\text{-}P3HT}$ following previously reported methods.[49,59,60] The analysis shows that 48% P3HT is converted into the H-aggregate state after aging, which is comparable to previously reported values

DOI: 10.1021/acsapm.9b00653
ACS Appl. Polym. Mater. 2019, 1, 2943−2950

of ~50%.[15,58] The disappearance of the peak at 450 nm has been used as an indicator of the formation of purely (~100%) crystalline P3HT and as a reference to estimate the crystallinity of less crystalline samples.[61] Despite the discrepancy on the precise determination of P3HT crystallinity in solution, it is reasonable to conclude that aged P3HT formed following this approach shows significant crystallinity.

The P3HT NWs formed can be deposited onto glass substrates for solid-state UV−vis measurements through spin-coating (Figure 1b). Because of the dramatic reduction of the absorbance of P3HT NWs on the surface as compared to solution samples, the signal-to-noise ratio of the spectra decreases. Meanwhile, the absorption peaks of the undoped P3HT NWs assigned to the 0−0 and 0−1 transition are slightly shifted to 602 and 546 nm, respectively. The A_{0-0}/A_{0-1} ratio is 0.67, which is very close to the ratio in solution, implying that the H-aggregate character remains after deposition. Upon sequential doping with a 50 μg/mL F4TCNQ solution, the aggregate absorption peaks decrease, accompanied by the emergence of a broad absorption band above 650 nm. This is due to the formation of P3HT polarons as a result of integer charge transfer between P3HT and F4TCNQ.[49,62] The 768 and 850 nm peaks associated with absorption by F4TCNQ anions cannot be resolved as a result of the sensitivity limits of the instrumentation.[49,50,62,63] Despite this limitation, the progress of sequential doping upon increasing dopant concentration can be tracked by monitoring the absorbance at 768 nm, which can be attributed to doping products. In the inset of Figure 1b, the absorbance at 768 nm sharply increases as a function of F4TCNQ concentration and saturates at a solution concentration >250 μg/mL. As the dopant concentration further increases above 500 μg/mL, the absorbance between 550 and 615 nm increases. This is likely due to the absorbance attributed to excess neutral F4TCNQ (λ_{max} = 380 nm, Figure S2).

P3HT NWs were spin-coated onto ITO substrates for a detailed analysis of these nanostructures using AFM. In Figure 2a, a 5 × 5 μm^2 overview of pristine P3HT NWs shows high-aspect-ratio P3HT NWs on the order of several micrometers in length that are uniformly distributed on the surface and which form an interconnected NW network. According to statistical analyses, the average height of undoped P3HT NWs is around 3.3 nm with a surface coverage around 33% (Table 1). A similar morphology with evenly dispersed P3HT NWs is shown in the first pass topography results obtained by using KPFM (Figure 2b), while the higher resolution image highlights the areas where multiple NWs overlap. Six cross-sectional height profiles of random isolated NWs marked with dotted lines were sampled (Figure 3 and Table 2). Because the statistical average thickness of P3HT NWs is around 3.3 nm,

Table 1. Quantities of Undoped and Doped P3HT Nanowire Networks[a]

	NWs			Excess Dopant		
Statistics	Average Height (nm)	RMS (nm)	Surface Coverage (%)	Average Height (nm)	RMS (nm)	Surface Coverage (%)
Undoped	3.3	1.8	33			
250 μg/mL	4.3	2.1	34			
1 mg/mL	4.8	2.9	31	18.4	5.5	10

[a]Note that in 1 mg/mL doped cases a significant presence of excessive dopant was observed on the surface. Therefore, surface coverage includes P3HT NW networks and excess dopant.

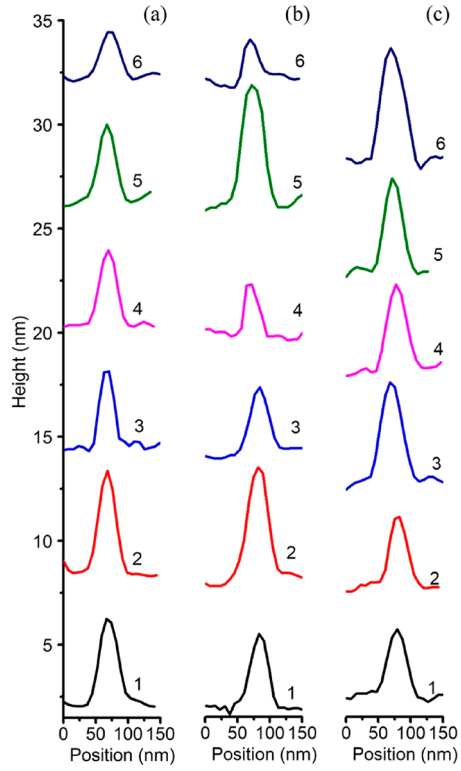

Figure 3. Typical cross-section height profiles of P3HT NWs on ITO substrate as marked by dotted lines in panels Figures 2b, 2e, and 2h, associated with panel (a) as-deposited, (b) sequentially doped with 250 μg/mL F4TCNQ, and (c) sequentially doped with 1 mg/mL F4TCNQ, respectively.

Table 2. Summary on the Heights of P3HT NWs on ITO Substrate as Marked by Dotted Lines in Figures 2b, 2e, and 2h

	Height (nm)					
NWs Sampling	1	2	3	4	5	6
Undoped	4.0	4.9	3.7	3.6	3.8	2.3
250 μg/mL	3.6	5.2	3.0	2.5	5.8	2.6
1 mg/mL	3.3	3.4	4.7	4.2	4.5	5.4

the NW network largely consists of double and triple layers. Interestingly, unlike our previous report on P3HT nanowhiskers where P3HT monolayers were more common,[29] no monolayer is observed here. This phenomenon can likely be attributed to the relatively long aging time of 18 h during which P3HT monolayers aggregate into more stable multilayered structures. No multilayered structures thicker than quadruple layers are observed, which may originate from the low P3HT concentration of 60 μg/mL.

When a moderate amount of F4TCNQ (i.e., 250 μg/mL) was applied to the pristine P3HT NWs, the overall network-like morphology remains intact (Figure 2d). Therefore, sequential doping does not drastically interfere with the structure of the nanostructures, which helps to preserve the crystallinity and domain orientation.[6−8] From the data in Table 1, the average thickness of the moderately doped P3HT NWs is about 4.3 nm, which is about 1 nm larger than the pristine

DOI: 10.1021/acsapm.9b00653
ACS Appl. Polym. Mater. 2019, 1, 2943−2950

NWs. Upon applying a larger amount of F4TCNQ (i.e., 1 mg/mL), dot-like features with submicrometer size can be observed on the surface (Figure 2g), which are attributed to neutral dopant. The excess dopant on the surface not only increases the average thickness of the NWs by about 1.5 nm but also introduces an additional surface coverage of about 10% (Table 1). Despite the drastic difference in the overall morphology between moderately doped and excessively doped surfaces, the surface coverage of the P3HT NWs remain at about 33%, confirming the minor effect associated with sequential doping on the existing structures. However, because of dopant deposition, the sampled cross-section heights of NWs increase in both doped cases (Table 2), resulting in an increase of layer thicknesses when compared to undoped NWs. The precise location where the F4TCNQ dopant resides within P3HT film remains elusive. From grazing-incidence wide-angle X-ray scattering (GIWAXS) studies on P3HT films derived from conventional mixed solution doping, Duong et al. first reported that the in-plane (010) peak at $q \sim 1.65$ Å^{-1}, which corresponds to $\pi-\pi$ spacing of 3.81 Å, splits into two peaks when sufficient doping of P3HT is achieved in solution.[63] Méndez et al. suggested the shifts of the (010) peaks can be attributed to the intercalation of dopants into the $\pi-\pi$ stacks of the P3HT backbones as a result of the formation of P3HT/F4TCNQ mixed cocrystallite phase from mixed solution doping.[64] However, according to Scholes et al., the intercalation of F4TCNQ into the P3HT π-stacks is not evident in both mixed solution and sequential doping methods.[7] Instead, they claimed that the change in $\pi-\pi$ spacing is due to the incorporation of the dopant into lamellar domains regardless of doping methods (solution mixing or sequential doping), which not only shifts side chain packing but also alters the $\pi-\pi$ stacking due to the dopant-induced interchain delocalization of polarons, which futher results in pulling adjacent polymer chains closer.[7] Despite the ongoing discussion on whether the dopant intercalates into $\pi-\pi$ stacks in P3HT films, the doping approach in this work may not lead to the infiltration of dopants into π-stacks because orthogonal solvents such as acetonitrile have a minimal swelling effect on the crystalline phase of P3HT.[8] Thus, intercalation of dopants into π-stacks of P3HT NWs during sequential doping seems unlikely. Additionally, upon doping, the shift of (100) peaks to the lower q region (increased lamellar d spacing) in GIWAXS indicates the possible incorporation of dopants into the lamellar region.[7,50,63,64] Based on this, the F4TCNQ dopant could reside in the internal lamellar regions of P3HT NWs through lateral diffusion or on the top surface of the NWs. The accurate determination of the dopant position with respect to the well-dispersed P3HT NWs is beyond the spatial resolving capability of our instrumentation.

Figure 2c highlights the CPD of undoped P3HT NWs. The imaging contrast presents a distinguishable separation of CPD values of NWs and the ITO background, resulting in a bimodal distribution in the CPD histogram as shown in Figure 4a. However, the CPD peak of P3HT NWs is 10 mV higher than the peak of the ITO reference (Figure 4a), indicating a slightly higher work function of the undoped P3HT NWs on ITO. Upon moderate doping (i.e., 250 μg/mL), CPD imaging of the doped P3HT NWs becomes featureless (Figure 2f). The CPD peak of P3HT NWs shifts to lower values and becomes indistinguishable to the ITO substrate (Figure 4b). When the P3HT NWs are excessively doped (i.e., 1 mg/mL), the CPD of P3HT NWs remains featureless while the excessive neutral

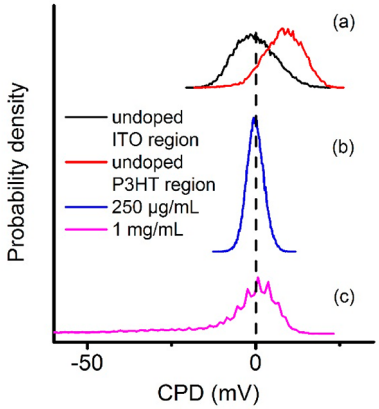

Figure 4. CPD histograms of (a) undoped P3HT NWs, (b) NWs sequentially doped with 250 μg/mL F4TCNQ, and (c) P3HT NWs sequentially doped with 1 mg/mL F4TCNQ, which corresponding to the CPD image as shown in Figures 2c, 2f, and 2i, respectively. The average CPD value of ITO is deliberately shifted to zero in all scenarios as an internal reference.

dopant shows significantly reduced CPD readings (Figure 2i). These lower CPD values result in an extended tail in the CPD histogram in the excessively doped case (Figure 4c). CPD profiles of marked cross sections in Figure 2i confirm the lower CPD values ranging from −20 to around −100 mV (Figure S3). This observation is qualitatively consistent with our previous report on the doping of ultrathin P3HT films,[65] in which KPFM imaging shows lower CPD values of −50 mV throughout the doped film in the presence of an excessive amount of dopant, while the CPD value of the film approaches that of the ITO reference when excessive dopant is removed by acetonitrile.

P3HT NWs can be deposited on quartz substrates for the measurements of conductivity by the same spin-coating method used in the preparation of AFM samples. In Figure 5a, a similar morphology of P3HT NWs with a surface coverage of ∼30% can be achieved. A summary of the statistics on the morphological parameters of undoped and doped P3HT NWs on quartz substrates can be found in Table S1. The average thickness of P3HT NWs on quartz substrates is 3.3 nm, close to that on ITO substrates. Upon doping by 250 μg/mL F4TCNQ, the thickness increases by 2 nm, larger than the ∼1 nm increment on ITO. While this difference might originate from differences in the substrate, it is within the 2 nm RMS of both undoped and doped P3HT. The $I-V$ curves of both undoped and doped samples are shown in Figure S4. The average conductivity of moderately doped P3HT is about 0.27 S/cm, which is significantly higher than 1.64×10^{-5} S/cm of undoped P3HT. Depending on molecular weight, regioregularity, solvent, or preparation methods, the electrical conductivity of pristine P3HT films is around $10^{-6}-10^{-4}$ S/cm.[8,57,62,63,65,66] The conductivity of the pristine P3HT NW network is within the range of values reported in the literature. For doped P3HT, the conductivity of films prepared from mixed solution doping ranges from 0.1 to 1 S/cm,[63,66−68] and that of sequentially doped P3HT films is shown to be 1−10 S/cm.[6,8,57] The conductivity of moderately doped P3HT NW networks is lower compared to a typical sequentially doped film.[65] It has been suggested that the infiltration of F4TCNQ into the amorphous region of P3HT film facilitates the segregation of dopant anions and charge transport pathways of

DOI: 10.1021/acsapm.9b00653
ACS Appl. Polym. Mater. 2019, 1, 2943−2950

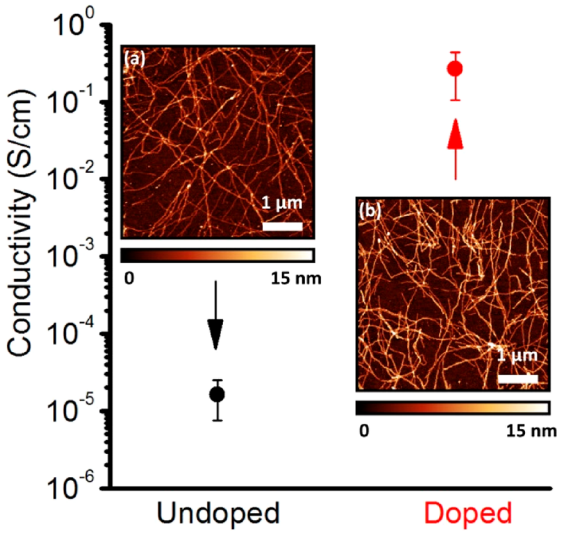

Figure 5. Conductivity of undoped and moderately doped P3HT NW network on a quartz substrate with prefabricated interdigitated Au electrodes. Inset (a) represents a 5 × 5 μm^2 scan of undoped P3HT network while inset (b) reveals the morphology of the doped network. Note that the moderately doped P3HT network can be prepared by spin-coating a 250 μg/mL F4TCNQ onto a pristine preformed P3HT NW film at 3000 rpm.

P3HT polarons, which may account for the higher conductivity of the sequentially doped P3HT film compared to mixed solution doping, particularly at lower doping levels.[8] Owing to the insignificant presence of amorphous P3HT regions in the NW networks, infiltration of F4TCNQ into highly ordered P3HT NW networks might be limited. In addition, because most of the nanowires are only a few nanometers thick, the diffusion of dopant in the doping of P3HT nanowires will play a much smaller role than in the doping for bulk films, where dopant molecules need to diffuse through thicknesses up to hundreds of nanometers or higher with substantial amount of amorphous domains. As previously mentioned, the most probable location of the dopant may be restricted to the lamellar region in the side chain direction or the top layer. This might hamper the overall doping level of P3HT NWs, which is consistent with the relatively lower conductivity as compared to the values obtained from typical sequential doping of a P3HT thin film.

CONCLUSION

A well-dispersed P3HT NW network was successfully prepared using an ultralow concentration of P3HT on a variety of substrates with ∼33% coverage. The average thickness is ∼3.3 nm, indicating that the majority of P3HT NWs are double- or triple-layer. The overall thickness of NW feature upon moderate doping (i.e., 250 μg/mL F4TCNQ) increases by 1−2 nm. A high concentration of dopant results in dot-like features on the surface of the film, which can be associated with excess neutral dopant dried out after the sequential doping process. These dot-like features have a broad distribution of CPD values well below the value of ITO, which is significantly different from the CPD of undoped NWs (∼10 mV) and moderately doped NWs (∼0 mV). The in-plane conductivities of undoped (1.64×10^{-5} S/cm) and doped P3HT NW networks (0.27 S/cm) demonstrate 4 orders of magnitude increase upon moderate doping of the highly ordered P3HT NW network. This proved that effective doping is still possible without a significant presence of amorphous domains that typically exist in P3HT thin films. However, this result is still lagging behind conducting nanofibers based on small molecules that show metallic charge transport behavior with conductivities significantly above 10 S/cm.[69,70] The possible locations of the dopant molecules include the lamellar region of the side chains or on the top layer. These results strengthen the understanding of doping of P3HT NW networks and shed light on improved design guidelines toward nanowire-based conjugated polymer devices.

ASSOCIATED CONTENT

Supporting Information

The Supporting Information is available free of charge on the ACS Publications website at DOI: 10.1021/acsapm.9b00653.

Deconvolution of the UV−vis spectrum of aged P3HT solution, UV−vis spectrum of pure F4TCNQ dopant, contact potential difference (CPD) profiles, *I*−*V* curves, and statistical quantities of undoped and doped P3HT NW networks (PDF)

AUTHOR INFORMATION

Corresponding Author

*E-mail song.guo@usm.edu.

ORCID

Jason D. Azoulay: 0000-0003-0138-5961

Song Guo: 0000-0002-3457-4331

Notes

The authors declare no competing financial interest.

ACKNOWLEDGMENTS

This work was supported by a National Science Foundation CAREER award (NSF DMR-1554841). L.H., J.L., and J.D.A. acknowledge support from the National Science Foundation (OIA-1632825, OIA-1757220, and DGE-1449999).

REFERENCES

(1) Lüssem, B.; Keum, C.-M.; Kasemann, D.; Naab, B.; Bao, Z.; Leo, K. Doped organic transistors. *Chem. Rev.* **2016**, *116* (22), 13714−13751.

(2) Xu, Y.; Sun, H.; Liu, A.; Zhu, H.-H.; Li, W.; Lin, Y.-F.; Noh, Y.-Y. Doping: A Key Enabler for Organic Transistors. *Adv. Mater.* **2018**, *30* (46), 1801830.

(3) Yoo, S. J.; Kim, J. J. Charge transport in electrically doped amorphous organic semiconductors. *Macromol. Rapid Commun.* **2015**, *36* (11), 984−1000.

(4) Reineke, S.; Lindner, F.; Schwartz, G.; Seidler, N.; Walzer, K.; Lüssem, B.; Leo, K. White organic light-emitting diodes with fluorescent tube efficiency. *Nature* **2009**, *459* (7244), 234.

(5) Kao, C. Y.; Lee, B.; Wielunski, L. S.; Heeney, M.; McCulloch, I.; Garfunkel, E.; Feldman, L. C.; Podzorov, V. Doping of conjugated polythiophenes with alkyl silanes. *Adv. Funct. Mater.* **2009**, *19* (12), 1906−1911.

(6) Scholes, D. T.; Hawks, S. A.; Yee, P. Y.; Wu, H.; Lindemuth, J. R.; Tolbert, S. H.; Schwartz, B. J. Overcoming Film Quality Issues for Conjugated Polymers Doped with F4TCNQ by Solution Sequential Processing: Hall Effect, Structural, and Optical Measurements. *J. Phys. Chem. Lett.* **2015**, *6* (23), 4786−4793.

(7) Scholes, D. T.; Yee, P. Y.; Lindemuth, J. R.; Kang, H.; Onorato, J.; Ghosh, R.; Luscombe, C. K.; Spano, F. C.; Tolbert, S. H.; Schwartz, B. J. The Effects of Crystallinity on Charge Transport and the Structure of Sequentially Processed F4TCNQ Doped Conjugated Polymer Films. *Adv. Funct. Mater.* **2017**, *27* (44), 1702654.

DOI: 10.1021/acsapm.9b00653
ACS Appl. Polym. Mater. 2019, 1, 2943−2950

(8) Jacobs, I. E.; Aasen, E. W.; Oliveira, J. L.; Fonseca, T. N.; Roehling, J. D.; Li, J.; Zhang, G.; Augustine, M. P.; Mascal, M.; Moulé, A. J. Comparison of solution-mixed and sequentially processed P3HT:F4TCNQ films: effect of doping-induced aggregation on film morphology. *J. Mater. Chem. C* **2016**, *4* (16), 3454−3466.
(9) Dang, M. T.; Hirsch, L.; Wantz, G.; Wuest, J. D. Controlling the Morphology and Performance of Bulk Heterojunctions in Solar Cells. Lessons Learned from the Benchmark Poly(3-hexylthiophene):[6,6]-Phenyl-C61-butyric Acid Methyl Ester System. *Chem. Rev.* **2013**, *113* (5), 3734−3765.
(10) Mas-Torrent, M.; Rovira, C. Role of Molecular Order and Solid-State Structure in Organic Field-Effect Transistors. *Chem. Rev.* **2011**, *111* (8), 4833−4856.
(11) Sirringhaus, H. 25th Anniversary Article: Organic Field-Effect Transistors: The Path Beyond Amorphous Silicon. *Adv. Mater.* **2014**, *26* (9), 1319−1335.
(12) Wang, C.; Dong, H.; Hu, W.; Liu, Y.; Zhu, D. Semiconducting π-Conjugated Systems in Field-Effect Transistors: A Material Odyssey of Organic Electronics. *Chem. Rev.* **2012**, *112* (4), 2208−2267.
(13) Hourani, W.; Rahimi, K.; Botiz, I.; Koch, F. P. V.; Reiter, G.; Lienerth, P.; Heiser, T.; Bubendorff, J.-L.; Simon, L. Anisotropic charge transport in large single crystals of π-conjugated organic molecules. *Nanoscale* **2014**, *6* (9), 4774−4780.
(14) Rahimi, K.; Botiz, I.; Agumba, J. O.; Motamen, S.; Stingelin, N.; Reiter, G. Light absorption of poly(3-hexylthiophene) single crystals. *RSC Adv.* **2014**, *4* (22), 11121−11123.
(15) Rahimi, K.; Botiz, I.; Stingelin, N.; Kayunkid, N.; Sommer, M.; Koch, F. P. V.; Nguyen, H.; Coulembier, O.; Dubois, P.; Brinkmann, M.; Reiter, G. Controllable processes for generating large single crystals of poly(3-hexylthiophene). *Angew. Chem., Int. Ed.* **2012**, *51* (44), 11131−11135.
(16) Lobov, G. S.; Zhao, Y.; Marinins, A.; Yan, M.; Li, J.; Sugunan, A.; Thylén, L.; Wosinski, L.; Östling, M.; Toprak, M. S.; Popov, S. Size Impact of Ordered P3HT Nanofibers on Optical Anisotropy. *Macromol. Chem. Phys.* **2016**, *217* (9), 1089−1095.
(17) Lobov, G. S.; Zhao, Y.; Marinins, A.; Yan, M.; Li, J.; Toprak, M. S.; Sugunan, A.; Thylen, L.; Wosinski, L.; Östling, M.; Popov, S. Electric field induced optical anisotropy of P3HT nanofibers in a liquid solution. *Opt. Mater. Express* **2015**, *5* (11), 2642−2647.
(18) McFarland, F. M.; Liu, X.; Zhang, S.; Tang, K.; Kreis, N. K.; Gu, X.; Guo, S. Electric field induced assembly of macroscopic fibers of poly (3-hexylthiophene). *Polymer* **2018**, *151*, 56−64.
(19) Xi, Y.; Pozzo, L. D. Electric field directed formation of aligned conjugated polymer fibers. *Soft Matter* **2017**, *13* (21), 3894−3908.
(20) Ye, Z.; Yang, X.; Cui, H.; Qiu, F. Nanowires with unusual packing of poly(3-hexylthiophene)s induced by electric fields. *J. Mater. Chem. C* **2014**, *2* (33), 6773−6780.
(21) Chen, J.-Y.; Kuo, C.-C.; Lai, C.-S.; Chen, W.-C.; Chen, H.-L. Manipulation on the morphology and electrical properties of aligned electrospun nanofibers of poly (3-hexylthiophene) for field-effect transistor applications. *Macromolecules* **2011**, *44* (8), 2883−2892.
(22) Chen, J.-Y.; Wu, H.-C.; Chiu, Y.-C.; Lin, C.-J.; Tung, S.-H.; Chen, W.-C. Electrospun Poly(3-hexylthiophene) Nanofibers with Highly Extended and Oriented Chains Through Secondary Electric Field for High-Performance Field-Effect Transistors. *Adv. Electron. Mater.* **2015**, *1* (1−2), 1400028.
(23) González, R.; Pinto, N. J. Electrospun poly(3-hexylthiophene-2,5-diyl) fiber field effect transistor. *Synth. Met.* **2005**, *151* (3), 275−278.
(24) Lee, S.; Moon, G. D.; Jeong, U. Continuous production of uniform poly(3-hexylthiophene) (P3HT) nanofibers by electrospinning and their electrical properties. *J. Mater. Chem.* **2009**, *19* (6), 743−748.
(25) Lee, S. W.; Lee, H. J.; Choi, J. H.; Koh, W. G.; Myoung, J. M.; Hur, J. H.; Park, J. J.; Cho, J. H.; Jeong, U. Periodic Array of Polyelectrolyte-Gated Organic Transistors from Electrospun Poly(3-hexylthiophene) Nanofibers. *Nano Lett.* **2010**, *10* (1), 347−351.
(26) Liu, H.; Reccius, C. H.; Craighead, H. G. Single electrospun regioregular poly(3-hexylthiophene) nanofiber field-effect transistor. *Appl. Phys. Lett.* **2005**, *87* (25), 253106.
(27) Samitsu, S.; Shimomura, T.; Ito, K. Nanofiber preparation by whisker method using solvent-soluble conducting polymers. *Thin Solid Films* **2008**, *516* (9), 2478−2486.
(28) Sarker, B. K.; Liu, J.; Zhai, L.; Khondaker, S. I. Fabrication of Organic Field Effect Transistor by Directly Grown Poly(3-Hexylthiophene) Crystalline Nanowires on Carbon Nanotube Aligned Array Electrode. *ACS Appl. Mater. Interfaces* **2011**, *3* (4), 1180−1185.
(29) McFarland, F. M.; Brickson, B.; Guo, S. Layered poly (3-hexylthiophene) nanowhiskers studied by atomic force microscopy and kelvin probe force microscopy. *Macromolecules* **2015**, *48* (9), 3049−3056.
(30) Han, Y.; Guo, Y.; Chang, Y.; Geng, Y.; Su, Z. Chain Folding in Poly(3-hexylthiophene) Crystals. *Macromolecules* **2014**, *47* (11), 3708−3712.
(31) Guo, Y.; Ma, X.; Su, Z. Interfacial interactions between poly(3-hexylthiophene) and substrates. *Macromolecules* **2013**, *46* (7), 2733−2739.
(32) Guo, Y.; Jiang, L.; Ma, X.; Hu, W.; Su, Z. Poly(3-hexylthiophene) monolayer nanowhiskers. *Polym. Chem.* **2013**, *4* (16), 4308−4311.
(33) Liu, J.; Zou, J.; Zhai, L. Bottom-up Assembly of Poly(3-hexylthiophene) on Carbon Nanotubes: 2D Building Blocks for Nanoscale Circuits. *Macromol. Rapid Commun.* **2009**, *30* (16), 1387−1391.
(34) Liu, J.; Arif, M.; Zou, J.; Khondaker, S. I.; Zhai, L. Controlling Poly(3-hexylthiophene) Crystal Dimension: Nanowhiskers and Nanoribbons. *Macromolecules* **2009**, *42* (24), 9390−9393.
(35) Arif, M.; Liu, J.; Zhai, L.; Khondaker, S. I. Poly(3-hexylthiophene) crystalline nanoribbon network for organic field effect transistors. *Appl. Phys. Lett.* **2010**, *96* (24), 243304.
(36) Ma, X.; Guo, Y.; Wang, T.; Su, Z. Scanning tunneling microscopy investigation of self-assembled poly(3-hexylthiophene) monolayer. *J. Chem. Phys.* **2013**, *139* (1), 014701.
(37) Merlo, J. A.; Frisbie, C. D. Field effect transport and trapping in regioregular polythiophene nanofibers. *J. Phys. Chem. B* **2004**, *108* (50), 19169−19179.
(38) Merlo, J. A.; Frisbie, C. D. Field effect conductance of conducting polymer nanofibers. *J. Polym. Sci., Part B: Polym. Phys.* **2003**, *41* (21), 2674−2680.
(39) Dierckx, W.; Oosterbaan, W. D.; Bolsée, J.-C.; Cardinaletti, I.; Maes, W.; Boyen, H.-G.; D'Haen, J.; Nesladek, M.; Manca, J. Organic phototransistors using poly (3-hexylthiophene) nanofibres. *Nanotechnology* **2015**, *26* (6), 065201.
(40) Bolsée, J.-C.; Oosterbaan, W. D.; Lutsen, L.; Vanderzande, D.; Manca, J. CAFM on conjugated polymer nanofibers: Capable of assessing one fiber mobility. *Org. Electron.* **2011**, *12* (12), 2084−2089.
(41) Bolsée, J. C.; Oosterbaan, W. D.; Lutsen, L.; Vanderzande, D.; Manca, J. The importance of bridging points for charge transport in webs of conjugated polymer nanofibers. *Adv. Funct. Mater.* **2013**, *23* (7), 862−869.
(42) Samitsu, S.; Shimomura, T.; Heike, S.; Hashizume, T.; Ito, K. Field-effect carrier transport in poly(3-alkylthiophene) nanofiber networks and isolated nanofibers. *Macromolecules* **2010**, *43* (19), 7891−7894.
(43) Samitsu, S.; Shimomura, T.; Heike, S.; Hashizume, T.; Ito, K. Effective production of poly(3-alkylthiophene) nanofibers by means of whisker method using anisole solvent: structural, optical, and electrical properties. *Macromolecules* **2008**, *41* (21), 8000−8010.
(44) Zhou, X.; Pfeiffer, M.; Blochwitz, J.; Werner, A.; Nollau, A.; Fritz, T.; Leo, K. Very-low-operating-voltage organic light-emitting diodes using a p-doped amorphous hole injection layer. *Appl. Phys. Lett.* **2001**, *78* (4), 410−412.
(45) Pfeiffer, M.; Beyer, A.; Fritz, T.; Leo, K. Controlled doping of phthalocyanine layers by cosublimation with acceptor molecules: A

DOI: 10.1021/acsapm.9b00653
ACS Appl. Polym. Mater. 2019, 1, 2943−2950

systematic Seebeck and conductivity study. *Appl. Phys. Lett.* **1998**, *73* (22), 3202−3204.
(46) Kivala, M.; Boudon, C.; Gisselbrecht, J.-P.; Enko, B.; Seiler, P.; Müller, I. B.; Langer, N.; Jarowski, P. D.; Gescheidt, G.; Diederich, F. Organic Super-Acceptors with Efficient Intramolecular Charge-Transfer Interactions by [2 + 2] Cycloadditions of TCNE, TCNQ, and F4-TCNQ to Donor-Substituted Cyanoalkynes. *Chem. - Eur. J.* **2009**, *15* (16), 4111−4123.
(47) Gao, Z. Q.; Mi, B. X.; Xu, G. Z.; Wan, Y. Q.; Gong, M. L.; Cheah, K. W.; Chen, C. H. An organic p-type dopant with high thermal stability for an organic semiconductor. *Chem. Commun.* **2008**, No. 1, 117−119.
(48) Gao, W.; Kahn, A. Controlled p-doping of zinc phthalocyanine by coevaporation with tetrafluorotetracyanoquinodimethane: A direct and inverse photoemission study. *Appl. Phys. Lett.* **2001**, *79* (24), 4040−4042.
(49) Wang, C.; Duong, D. T.; Vandewal, K.; Rivnay, J.; Salleo, A. Optical measurement of doping efficiency in poly(3-hexylthiophene) solutions and thin films. *Phys. Rev. B: Condens. Matter Mater. Phys.* **2015**, *91* (8), 085205.
(50) Muller, L.; Nanova, D.; Glaser, T.; Beck, S.; Pucci, A.; Kast, A. K.; Schroder, R. R.; Mankel, E.; Pingel, P.; Neher, D.; Kowalsky, W.; Lovrincic, R. Charge-transfer−solvent interaction predefines doping efficiency in p-doped P3HT films. *Chem. Mater.* **2016**, *28* (12), 4432−4439.
(51) Clark, J.; Silva, C.; Friend, R. H.; Spano, F. C. Role of Intermolecular Coupling in the Photophysics of Disordered Organic Semiconductors: Aggregate Emission in Regioregular Polythiophene. *Phys. Rev. Lett.* **2007**, *98* (20), 206406.
(52) Spano, F. C.; Silva, C. H- and J-Aggregate Behavior in Polymeric Semiconductors. *Annu. Rev. Phys. Chem.* **2014**, *65* (1), 477−500.
(53) Spano, F. C. The Spectral Signatures of Frenkel Polarons in H- and J-Aggregates. *Acc. Chem. Res.* **2010**, *43* (3), 429−439.
(54) Spano, F. C. Modeling disorder in polymer aggregates: The optical spectroscopy of regioregular poly(3-hexylthiophene) thin films. *J. Chem. Phys.* **2005**, *122* (23), 234701.
(55) Louarn, G.; Trznadel, M.; Buisson, J. P.; Laska, J.; Pron, A.; Lapkowski, M.; Lefrant, S. Raman Spectroscopic Studies of Regioregular Poly(3-alkylthiophenes). *J. Phys. Chem.* **1996**, *100* (30), 12532−12539.
(56) Botta, C.; Luzzati, S.; Tubino, R.; Borghesi, A. Optical excitations of poly-3-alkylthiophene films and solutions. *Phys. Rev. B: Condens. Matter Mater. Phys.* **1992**, *46* (20), 13008−13016.
(57) Hynynen, J.; Kiefer, D.; Yu, L.; Kroon, R.; Munir, R.; Amassian, A.; Kemerink, M.; Müller, C. Enhanced Electrical Conductivity of Molecularly p-Doped Poly(3-hexylthiophene) through Understanding the Correlation with Solid-State Order. *Macromolecules* **2017**, *50* (20), 8140−8148.
(58) Clark, J.; Chang, J.-F.; Spano, F. C.; Friend, R. H.; Silva, C. Determining exciton bandwidth and film microstructure in polythiophene films using linear absorption spectroscopy. *Appl. Phys. Lett.* **2009**, *94* (16), 163306.
(59) McFarland, F. M.; Bonnette, L. R.; Acres, E. A.; Guo, S. The impact of aggregation on the p-doping kinetics of poly(3-hexylthiophene). *J. Mater. Chem. C* **2017**, *5* (23), 5764−5771.
(60) Turner, S. T.; Pingel, P.; Steyrleuthner, R.; Crossland, E. J. W.; Ludwigs, S.; Neher, D. Quantitative Analysis of Bulk Heterojunction Films Using Linear Absorption Spectroscopy and Solar Cell Performance. *Adv. Funct. Mater.* **2011**, *21* (24), 4640−4652.
(61) Oh, J. Y.; Shin, M.; Lee, T. I.; Jang, W. S.; Min, Y.; Myoung, J.-M.; Baik, H. K.; Jeong, U. Self-Seeded Growth of Poly(3-hexylthiophene) (P3HT) Nanofibrils by a Cycle of Cooling and Heating in Solutions. *Macromolecules* **2012**, *45* (18), 7504−7513.
(62) Pingel, P.; Neher, D. Comprehensive picture of p-type doping of P3HT with the molecular acceptor F4TCNQ. *Phys. Rev. B: Condens. Matter Mater. Phys.* **2013**, *87* (11), 115209.
(63) Duong, D. T.; Wang, C.; Antono, E.; Toney, M. F.; Salleo, A. The chemical and structural origin of efficient p-type doping in P3HT. *Org. Electron.* **2013**, *14* (5), 1330−1336.
(64) Méndez, H.; Heimel, G.; Winkler, S.; Frisch, J.; Opitz, A.; Sauer, K.; Wegner, B.; Oehzelt, M.; Röthel, C.; Duhm, S.; Többens, D.; Koch, N.; Salzmann, I. Charge-transfer crystallites as molecular electrical dopants. *Nat. Commun.* **2015**, *6*, 8560.
(65) Tang, K.; McFarland, F. M.; Travis, S.; Lim, J.; Azoulay, J. D.; Guo, S. Aggregation of P3HT as a preferred pathway for its chemical doping with F4-TCNQ. *Chem. Commun.* **2018**, *54* (84), 11925−11928.
(66) Yim, K.-H.; Whiting, G. L.; Murphy, C. E.; Halls, J. J. M.; Burroughes, J. H.; Friend, R. H.; Kim, J.-S. Controlling Electrical Properties of Conjugated Polymers via a Solution-Based p-Type Doping. *Adv. Mater.* **2008**, *20* (17), 3319−3324.
(67) Kiefer, D.; Yu, L.; Fransson, E.; Gómez, A.; Primetzhofer, D.; Amassian, A.; Campoy-Quiles, M.; Müller, C. A Solution-Doped Polymer Semiconductor:Insulator Blend for Thermoelectrics. *Adv. Sci.* **2017**, *4* (1), 1600203.
(68) Glaudell, A. M.; Cochran, J. E.; Patel, S. N.; Chabinyc, M. L. Impact of the Doping Method on Conductivity and Thermopower in Semiconducting Polythiophenes. *Adv. Energy Mater.* **2015**, *5* (4), 1401072.
(69) Faramarzi, V.; Niess, F.; Moulin, E.; Maaloum, M.; Dayen, J.-F.; Beaufrand, J.-B.; Zanettini, S.; Doudin, B.; Giuseppone, N. Light-triggered self-construction of supramolecular organic nanowires as metallic interconnects. *Nat. Chem.* **2012**, *4*, 485.
(70) Zhen, Y.; Inoue, K.; Wang, Z.; Kusamoto, T.; Nakabayashi, K.; Ohkoshi, S.-i.; Hu, W.; Guo, Y.; Harano, K.; Nakamura, E. Acid-Responsive Conductive Nanofiber of Tetrabenzoporphyrin Made by Solution Processing. *J. Am. Chem. Soc.* **2018**, *140* (1), 62−65.

DOI: 10.1021/acsapm.9b00653
ACS Appl. Polym. Mater. 2019, 1, 2943−2950